Available online at www.elixirpublishers.com (Elixir International Journal)

Condensed Matter Physics

Elixir Condensed Matter Phys. 163 (2022) 56047-56052

ISSN: 2229-712X

Photon-Assisted Transport Phenomenon in Graphene Nanoribbons: A Quasi-Classical Approach

M. Rabiu[1], D. Gyasi-Antwi[2], M. Amekpewu[1] P. K. Mensah[2], S. S. Abukari[3] and S. Y. Mensah[3]

[1]University for Development Studies, School of Engineering, Department of Physics, Tamale, Ghana.

[2]C. K. Tedam University of Technology and Applied Sciences, Department of Applied Physics Navrongo, Ghana.

[3]University of Cape Coast, Department of Physics, Laser and Fiber Optics Center, Cape Coast, Ghana.

ARTICLE INFO

Article history:

Received: 27 November 2021;

Received in revised form:

18 January 2022;

Accepted: 7 February 2022;

Keywords

Graphene Ribbon,

Current Density,

Bessel Function,

Photon-assisted Process.

ABSTRACT

A semi-classical Boltzmann transport model is developed to observe photon-assisted dynamics of induced carriers in the graphene nanoribbons. When the nanoribbons are subjected to a multi-frequency Alternating Current (ac) field and superimposed on by static Direct Current (dc) field, an unusual non-linear response of the system shows up at a rather strong drive force. The non-linearity in the photo-current allows for up-conversion necessary for low-frequency oscillators. Regions of positive differential conductivity are observed paving way for graphene to be operated as a small signal amplifier for Terahertz (THz) applications. The fractional photon-assisted phenomenon is also observed when the stark factor r > 1 and the ratio of the n-th harmonic to stark factor takes on half-integer values.

1. Introduction

Photon-assisted processes in systems are quantum phenomena in the presence of strong ac fields in which electrons can absorb (emit) one or several photons. The absorption (emission) of photons opens up new conduction channels in the system. The observation of photon assisted processes in solid-state materials is a central ingredient for terahertz (THz) generations. Photon-assisted peaks of up to 7 THz photons has been reported in (Zeuner, 1996) and can persist up to room temperature. Graphene is purely 2D material and has been tipped as a unique and wonder material since it demonstrates novel transport phenomena over conventional materials (Geim & Novoselov, 2007). Graphene nanoribbons have been suggested as a potential candidate for replacing electronic components in future nanoelectronics devices [(Geim & Novoselov, 2007), (Son, Cohen, & Louie, 2006)] due to the absence of gap opening by graphene sheets. This makes graphene ribbon a suitable candidate to examine photon-assisted processes in Dirac systems (Castro Neto, Guinea, Peres, Novoselov, & Geim, 2009), (Lurov, Gumbs, Roslyak, & D., 2011), (Trauzettel, Blanter, & Morpurgo, 2007). In rolled-up graphene ribbons (carbon nanotubes (CNTs)), photon-assisted processes occur because the current dynamics in the system can be seen as Bloch oscillations when an ac field is added to a dc field. A large ac amplitude opens up transport channels which can be seen as photon peaks. Regions of positive differential conductivity at certain ranges of the dc field is then formed. As a consequence, electric field domain suppression ideal for amplification of THz frequencies can be achieved (Seidu, 2011).

In this paper, we have developed a quasi-classical approximation to investigate the possibility of photon-assisted processes in the armchair and zigzag graphene nanoribbons motivated by the fact that photon-assisted tunnelling was studied quite recently (Lurov, Gumbs, Roslyak, & D., 2011), where low energy dispersion of electrons was used. Here, we explore not the tunnelling of Dirac electrons in graphene through barriers but the operation regions for possible THz amplification using the full tight binding dispersion. We will show that the Current-Voltage (I-V) characteristics demonstrate regions of positive differential conductivity where a graphene nanodevice can be operated as a small signal amplifier. We noted that a dynamical response of the carriers to THz radiation can depend on details of scattering processes, this effect could lead to the relaxation towards a thermal equilibrium which we relax here. Again, we ignore transient processes by assuming that $t >> \tau$ (Romanov, Romanova, & G., 2009).

The rest of the article is organized as follows; we derived the photon-assisted current density in section 2.1. Using the photon currents, we study the photon replicas and dynamic localization in the presence of monochromatic and biharmonic frequencies in section 2.2. I-V characteristic graphs are plotted and discussed in detail in section 3 and the paper finally concludes in section 4 outlying some further investigations.

2. Theory

Consider the motion of carriers in graphene upon application of multi-frequency external field. In nanoribbons, dynamics are localized along one direction plus quantization in the transverse direction. Carriers in the system are governed by the quasi-classical Boltzmann equation

$$\frac{\partial f(k,t)}{\partial t} + \frac{eE(t)}{\hbar}\frac{\partial f(k,t)}{\partial k} = \frac{\Delta f(k,t)}{\tau} \quad (1)$$

Where ħk is the carrier quasi-momentum and $\boldsymbol{\tau}$ is the relaxation of the system to equilibrium Fermi distribution, $\boldsymbol{f_0}$ after application of the field. Δf = (f - $\boldsymbol{f_0}$) is the deviation from non-equilibrium distribution. To study the optical response which gives rise to photo-assisted process, the nanoribbons to the external time-varying photon field.

$$\boldsymbol{E(t) = \sum_{j=0}^{N} E_j e^{i\omega t + i\alpha_j}} \quad (2)$$

The phase shift is defined as $\boldsymbol{\alpha_j = \omega_{j+1} - \omega}$. A static field corresponds to the j = 0 or $\boldsymbol{\omega_0 = \alpha = 0}$. The field amplitudes, $\boldsymbol{E_j}$ are responsible for the opening of new transport channels for THz gain.

Now, motivated by the quantization of the momentum along the transverse (zigzag, armchair) edge and in line with the consideration in references (Litvinov & Manasson, 2004), (Yan, Bao, & Zhao, 1998), (Ghosh, Kuznetsov, & Wilkins, 1997), (Zhao, 1991), (Kroemer, 2000), (Musa, Mensah, & Abukari, 2012) we expand in Fourier series, the Fermi distributions, f_0, f and the carrier energy, Ɛ as

$$\boldsymbol{f_0(k,\theta) = \sum_{s=1}^{N} \sum_{r\neq 0} f_{rs}\, \theta_s\, \delta(\theta_s - s\Delta\theta) e^{irkl}}, \quad (3)$$

$$\boldsymbol{f(k,\theta,t) = \sum_{s=1}^{N} \sum_{r\neq 0} f_{rs}\, \theta_s\, \delta(\theta_s - s\Delta\theta) \Phi_r(t) e^{irkl}}, \quad (4)$$

$$\boldsymbol{\mathcal{E}(k,\theta) = \gamma_0 \sum_{s=1}^{N} \sum_{r\neq 0} \mathcal{E}_{rs}\, \theta_s\, \delta(\theta_s - s\Delta\theta) e^{irkl}}, \quad (5)$$

here the Fourier coefficients are

$$\boldsymbol{f_{rs} = \frac{l}{2\pi s\Delta\theta} \int_{\pi/l}^{\pi/l} dk f_0(k,\theta) e^{-irkl}}$$

And

$$\boldsymbol{\mathcal{E}_{rs} = \frac{l}{2\pi\gamma_0} \int_{\pi/l}^{\pi/l} dk \mathcal{E}(k,\theta) e^{-irkl}}$$

With the help of equations (3), (4) and (5), the factor $\boldsymbol{\Phi_r}$ determining the non-equilibrium contribution can be determined by standard techniques.

$$\boldsymbol{\Phi_r(t) = \sum_{n_j,v_j=-\infty}^{\infty} J_{n_j}(r\beta_j) J_{n_j - v_j}(r\beta_j) \frac{e^{iv_j\omega_j t + iv_j\alpha_j}}{1 + i\tau(r\beta_0 + n_j\omega_j)}} \quad (6)$$

2.1 Photo-current density

To study photo-induced carrier transport in graphene, we observe the response of the system to the time-varying electric field. Because of this, we defined a time-dependent current density

$$\boldsymbol{j = \frac{g_s g_v e}{4\pi^2} \sum_{s=1}^{M} \int dk v(k,\theta_s) f(k,\theta_s,t)} \quad (7)$$

Where the velocity of the carriers is defined as $\boldsymbol{v = \delta\mathcal{E}/\hbar\delta k}$. Putting equation 6 into 4 and the result in equation 7 leads to the Orlov and Romanov expression

$$\boldsymbol{j = i \sum_{r=1}^{\infty} j_{0r} \left[\sum_{n_j,v_j=-\infty}^{\infty} \prod_{j=1}^{n} J_{n_j}(r\beta_j) J_{n_j - v_j}(r\beta_j) \frac{e^{iv_j\omega_j t + iv_j\alpha_j}}{1 + i\tau(r\beta_0 + n_j\omega_j)} + c.c \right]}, \quad (8)$$

where $J_n(x)$ are Bessel functions of n^{th} order.

$\boldsymbol{\beta_j = \frac{elE_j}{\hbar\omega}}$, $\boldsymbol{\beta_0 = \frac{elE_0}{\hbar}}$ and $\boldsymbol{j_0}$ is the peak current defined as

$$\boldsymbol{j_{0r} = \frac{2g_s g_v e\gamma_0}{\pi l\hbar} \Delta\theta \sum_{s=1}^{n} r\mathcal{E}_{rs} f_{rs}}$$

$\boldsymbol{\Delta\theta = \pi/N+1}$ $\boldsymbol{and\ l = \frac{\sqrt{3}a}{2}}$ for aGNR, $\boldsymbol{\Delta\theta = (2 + 1/s)\pi/N+1}$ and $\boldsymbol{l = a/2}$ for zGNR

To have a more simplified equation that describes the phenomenon we are considering,

we adopt the following definitions;

$\boldsymbol{\beta_0\tau = \frac{E_0}{E_{cr}}}$ $\boldsymbol{E_{cr} = \hbar/el\tau}$

$\boldsymbol{\beta_j = E_j/E_j^*}$ $\boldsymbol{E_j^* = \hbar\omega_j/el}$

With $\omega_j\tau = {E_j^*}/{E_{cr}}$. E^* is the electric field at which an electron emits or absorbs a quantum of energy of the photon when displaced by quasi-lattice period *l*. E_{cr} is, however, the critical field at which carriers get their peak velocity. With this choice of variables, we make the replacement $\beta_0\tau + n_j\omega_j\tau \to \frac{E_0}{E_{cr}} + n_j {E_j^*}/{E_{cr}}$ so that Eq. (8) becomes

$$j(t) = i\sum_{r=1}^{\infty} j_{0r}\left[\sum_{n_j,v_j=-\infty}^{\infty}\prod_{j=1}^{n} J_{n_j}\left(r\,{E_j}/{E_j^*}\right)J_{n_j-v_j}\left(r\,{E_j}/{E_j^*}\right)\right] x\, f\left(r\frac{E_0}{E_{cr}} + n_j\,{E_j^*}/{E_{cr}}\right)e^{iv_j\omega_j t + iv_j\alpha_j}\ , \quad (9)$$

where f(x) is the superposition of weighted photon replicas of pure dc differential current density. If the above equation is compared to the pure DC density in reference (Hyart, Alexeeva, Mattas, & Alekseev, 2009), (Hyart, Alekseev, & Thuneberg, Bloch Gain in dc-ac-driven semiconductor superlattices in the absence of electric domains, 2008) we see that the photon peaks are displaced by multiples of ${E^*}/{E_{cr}}$ with amplitudes of J_n^2. Note that if r = 1 and $n_j = 1$ the Bloch frequency, $\omega_B = \left({elE_0}/{\hbar}\right)$ associated with the static field will coincide with the applied frequency ω_j and no photon replicas can be seen. Therefore it is a requirement that $r \neq n_j$ *and* $n_j \neq 1$ if PAPs are to be observed. In the following section, we will consider two cases of Eq. (9); the monochromatic and bichromatic cases in the presence of the static electric field.

2.2 Large-signal dynamic localization and photon-assisted replicas

2.2.1 Graphene nanoribbon in monochromatic Field

When an ac field of frequency, ω is applied to the GNR, we have n = 1, $\omega_{j>1} = 0$ *and* $\alpha_j = 0$ in Eq. (9) which becomes

$$j = i\sum_{r=1}^{\infty}\frac{j_{0r}}{E}\left[\sum_{n,v=-\infty}^{\infty} J_n\left(r\,{E}/{E^*}\right)J_{n-v}\left(r\,{E}/{E^*}\right) f\left(r\frac{E_0}{E_{cr}} + n\,{E^*}/{E_{cr}}\right)\right]E\cos(v\omega t)\cdot \quad (10)$$

The coefficient of $E\cos(v\omega t)$ in Eq. (11) is an ac part of the drive field. It is seen as a large-signal dynamic conductivity at the derived harmonic frequency ω. The fundamental derived frequency is obtained by setting υ = ±1. To simplify the preceding equation further, we take υ = 0 to get cos ($v\omega t$) = 1, so that

$$j = i\sum_{r=1}^{\infty} j_{0r}\left[\sum_{n=-\infty}^{\infty} J_n^2\left(r\,{E}/{E^*}\right)f\left(r\frac{E_0}{E_{cr}} + n\,{E^*}/{E_{cr}}\right)\right] \quad (11)$$

2.2.2 Graphene nanoribbon in bichromatic Field

Now, for an applied field of frequencies, ω_1 *and* ω_2 we have n = 2 and $\omega_{j>2} = 0$. These set$\alpha_{j>1} = 0$. One can put $v_1 \neq 0$ *and* $v_2 \neq 0$ allowing Eq. (10) look like

$$j = i\sum_{r=1}^{\infty} j_{0r}\sum_{v_1,v_2=-\infty}^{\infty}\sum_{n_1,n_2=-\infty}^{\infty} J_{n_1}\left(r\,{E_1}/{E_1^*}\right)J_{n_1-v_1}\left(r\,{E_1}/{E_1^*}\right)J_{n_2}\left(r\,{E_2}/{E_2^*}\right) x\, J_{n_2-v_2}\left(r\,{E_1}/{E_1^*}\right) f\left(r\frac{E_0}{E_{cr}} + n_1\,{E_1^*}/{E_{cr}} + n_2\,{E_2^*}/{E_{cr}}\right)\cos(v_2\,\alpha) \quad (12)$$

We arrived at the last equation by allowing the two frequencies to be commensurable, i.e., $|v_1|\omega_1 = |v_2|\omega_2$ and periodic, i.e., with $\omega_2 = \mu\omega_1$ You can see references (Romanov, Romanova, & G., 2009) and references therein the case of non-commensurable frequencies. Further if $v_1 = 0$ *and* $v_2 = 0$ then a more simplified equation

$$j = i\sum_{r=1}^{\infty} j_{0r}\left[\sum_{n_1,n_2=-\infty}^{\infty} J_{n_1}^2\left(r\,{E_1}/{E_1^*}\right)J_{n_2}^2\left(r\,{E_2}/{E_2^*}\right) f\left(r\frac{E_0}{E_{cr}} + n_1\,{E_1^*}/{E_{cr}} + n_2\,{E_2^*}/{E_{cr}}\right)\right] \quad (13)$$

is obtained. A significant difference between the above two equations is the phase factor $\cos(v_2\,\alpha)$. Of course, among other differences, Eq. (13) will be an inversion of Eq. (12) for $\alpha \in \left[{\pi}/{2}, {3\pi}/{2}\right]$. The advantage of the biharmonic field over the monoharmonic field is that in the former, new local structures in the I-V characteristics become most pronounced. We shall see this in the following section.

3. Results and Discussions

The graphs in Fig.1 are $j - E_0$ the plot of Eq. (10) demonstrate the appearance of positive differential conductivity (PDC) regions at high applied frequencies, $\omega\tau \sim 10$. Particularly in AGNR, when the Bloch frequency associated with the bias field falls within the ranges $9.15\,\tau^{-1} < \omega_B < 10.9\,\tau^{-1}$,*l*$9.25\,\tau^{-1} < \omega_B < 20.65\,\tau^{-1}$*etc.*, NDC is greatly suppressed and the device can be operated effectively. This means the system is free from space charge instability. Any small signal passing through the ribbon no longer suffer from electrical domains and can thus easily get modified. The scenario is the same for ZGNR except that some operation points are hidden at large ${E_0}/{E^*}$ values. From the Figure, because the peaks show up at

$E_{cr}/_{E^*} + n > E_0/_{E^*}$ and the minima at $E_0/_{E^*} > n$, where n is the number of peaks, one can deduce a general range of bias field for best device operation to lie within $n < E_0/_{E^*} < n + E_{cr}/_{E^*}$ or $n\omega\tau < \omega_B\tau < n\omega\tau + 1$.

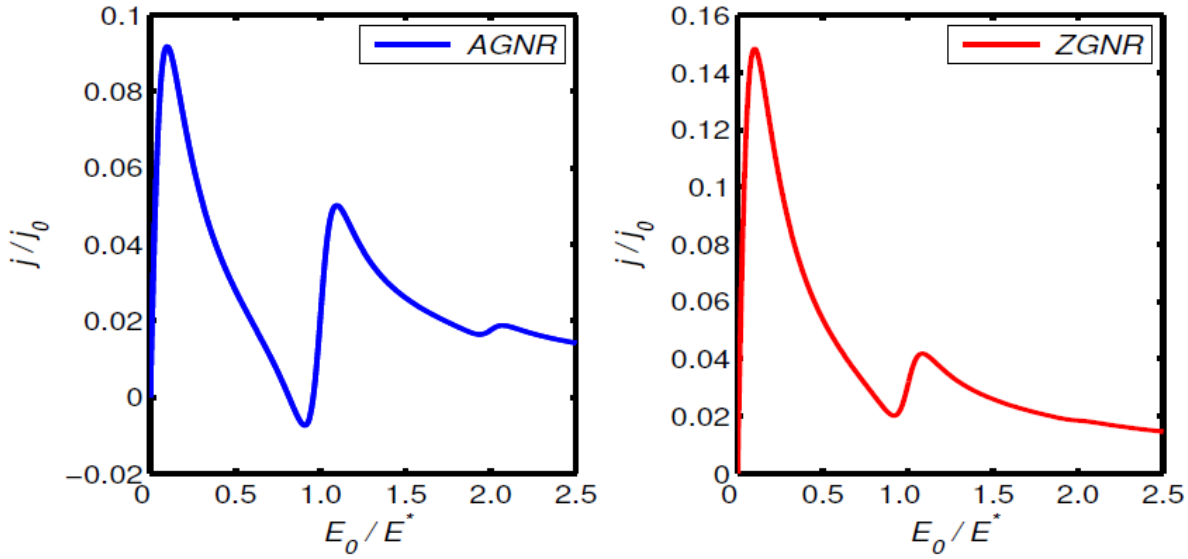

Figure 1. I-V characteristic showing regions of PDC for (left) armchair and (right) zigzag ribbons. ωτ = 10, $E = E^*$.

The behaviour of Eq. (11) is shown in Fig.2. PDC effect is observed at high even and odd harmonics. We chose υ = 2, υ = 3 and $\cos(\upsilon\alpha) = 1$.The two graphs are distinct, they are mirror reflections of each other. NDC in AGNR becomes PDC in ZGNR and vice-versa. It is clear from the two curves that depending on the sign of $\cos(\alpha)$ the operation ranges in one ribbon can be greater than the other. Photon-assisted peaks are shown in Fig.3 (blue) for aGNR. Multi-photon resonances appear when $r\omega_B\tau = n\omega\tau$ for an integer n. If n/r is the order of the Bessel functions with root coinciding with one of the $E/_{E^*}$ values in Fig (3), a dynamic localization is seen. Depending on how the ratio $E/_{E^*}$ is chosen, the localized charged carriers can extend the localization beyond its vicinity and thus affecting neighbouring centres. This might account for the decrease in neighbouring peak heights. The suppression at the first photon-assisted peak of the red curve is due to the combined destructive effect of ac-dc fields at $E_0 = E^*$. To observe new transport channels in graphene, we plot the high dynamic conductivity with $E/_{E^*}$ with μ = 2 in Fig.4. Transport processes are allowed at $E/_{E^*} = n$. This might be an indication that at high harmonics many more channels are opened up giving a way for proper direct signal rectification.

A very important phenomenon of fractional photon-assisted processes is obtained in graphene nanoribbon when the stark component r > 1 even though the integer photon assisted peaks are still more pronounced. In Fig.5 fractional peaks are formed at n/r = 0.5, 1.0, 1.5, 2.0,.

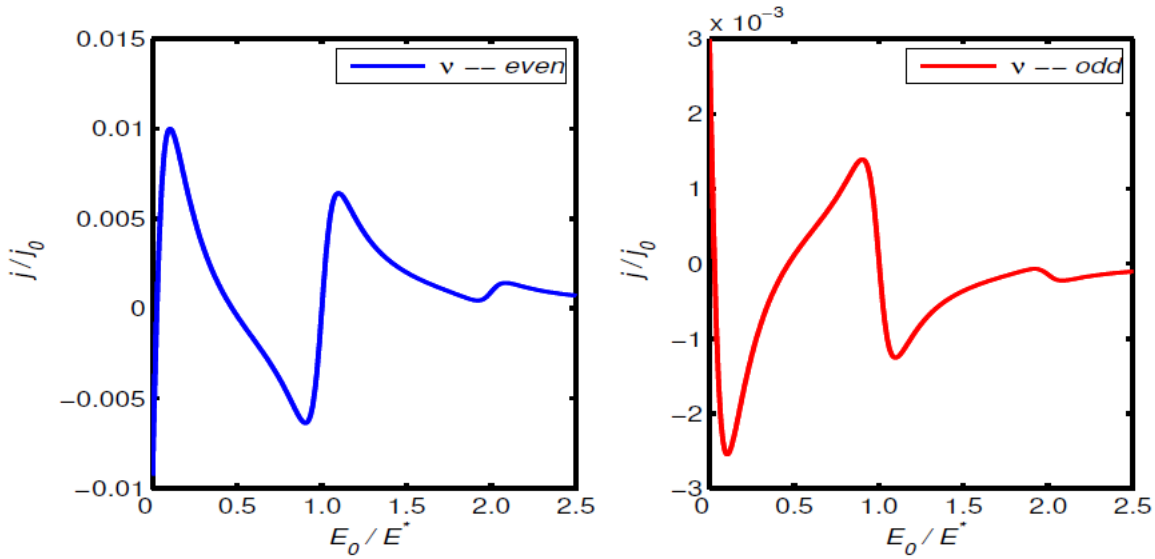

Figure 2. High-harmonic I-V characteristic showing regions of PDC at (left) even harmonics and (right) odd harmonics for AGNR. $\omega\tau = 10$, $E = 1.6E^*$.

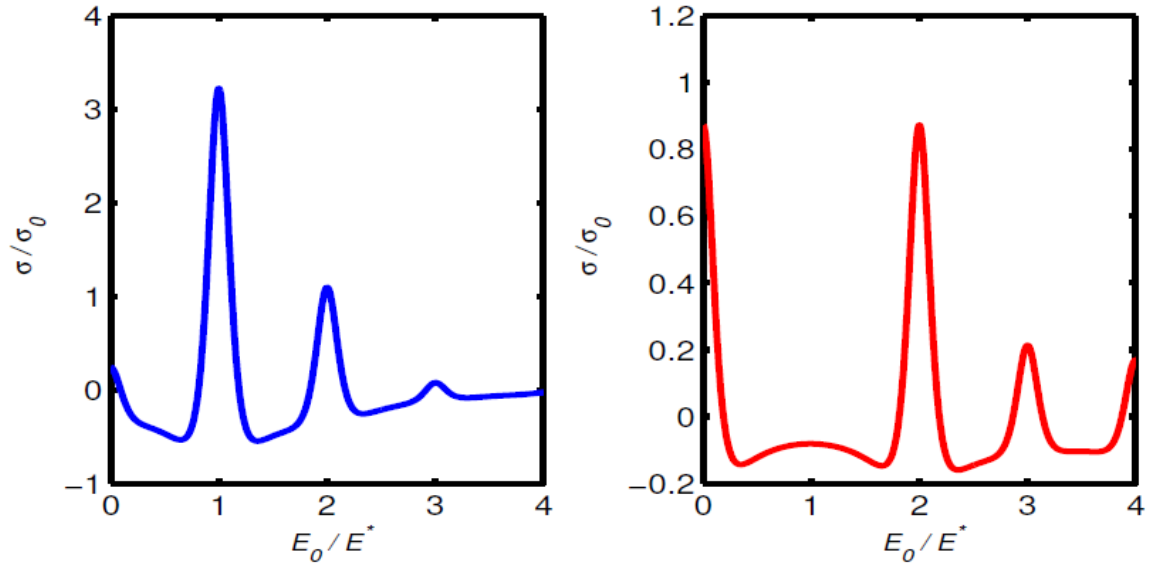

Figure 3. (blue) Photon-assisted peaks for $E = 2.0E^*$ (red) Photon-assisted peaks for $E = 5.0E^*$ Transport channels appear at $\omega_b = \omega, 2\omega, 3\omega, ...$

4. Conclusion

We have used the complete tight-binding spectrum of graphene to show the phenomenon of photon assisted processes and dynamic localization in graphene. A signature that may be responsible for rectification and amplification of ac fields. We found yet another quantum mechanical behaviour of graphene nanoribbons, a fractional photon-assisted process. We have suggested the use of our theoretical approach for studying terahertz generation and small signal amplification in graphene nanoelectronic devices

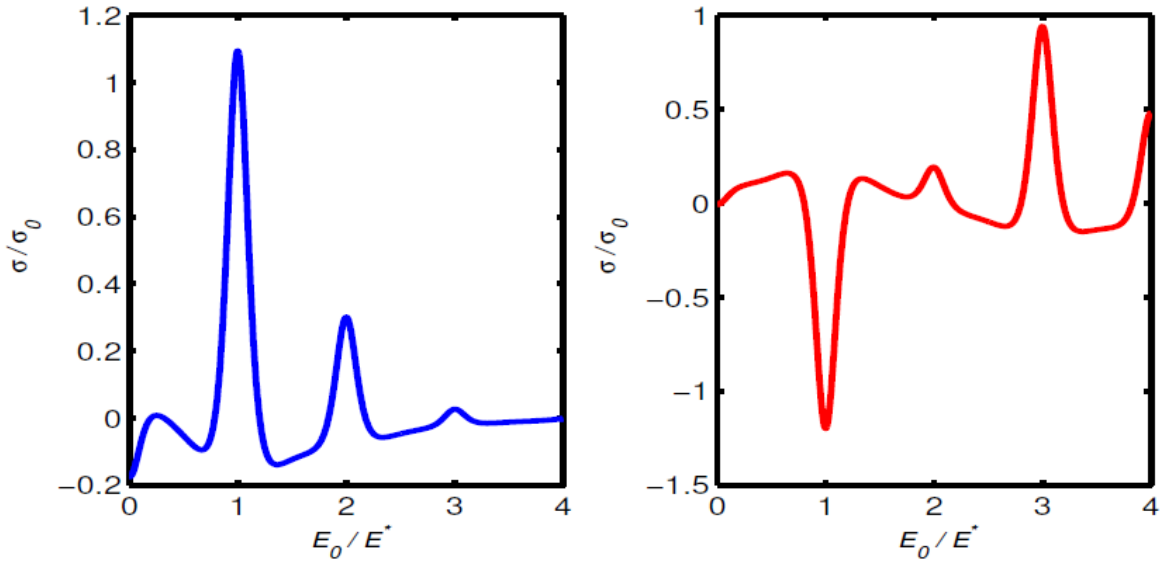

Figure 4. (blue) Photon-assisted peaks for $E = 2.5E^*$ (red) Photon-assisted peaks for $7.0E^*$. Transport channels appear at $\omega_B = \omega, 2\omega, 3\omega, ...$

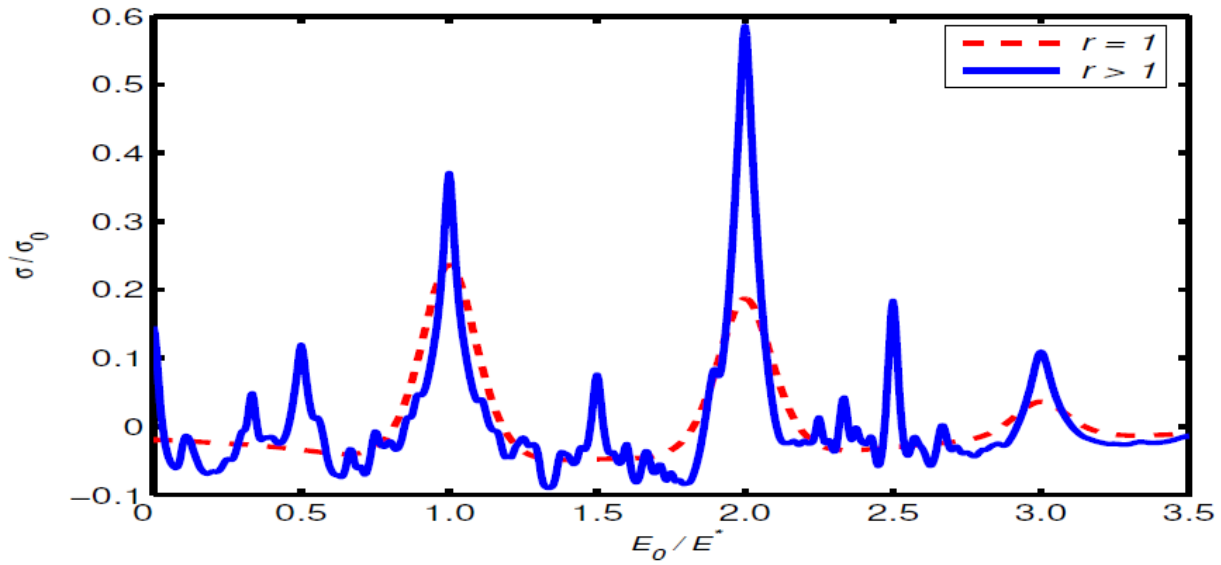

Figure 5. Fractional photon assisted process in graphene nanoribbon.

.

Authors' contributions

Conceived and designed the Work: Musah Rabiu, Daniel Gyasi-Antwi, Matthew Amekpewu, Philip Kwasi Mensah, S.S. Abukari, S.Y. Mensah

Analyzed the data: Musah Rabiu, Daniel Gyasi-Antwi, Matthew Amekpewu, Philip Kwasi Mensah, S.S. Abukari , S.Y. Mensah

Wrote the paper: Musah Rabiu, Daniel Gyasi-Antwi, Matthew Amekpewu, Philip Kwasi Mensah, S.S. Abukari , S.Y. Mensa

References

Castro Neto, A. H., Guinea, F., Peres, N. M., Novoselov, K. S., & Geim, A. K. (2009). The Electronic Properties of Graphene. Reviews of Modern Physics, 81(1), 109-162.

Geim, A. K., & Novoselov, K. (2007). The Rise of Graphene. Nature Materials, 6, 183-191.

Ghosh,A.W.,Kuznetsov,A.V.,&Wilkins, J. W. (1997).

Reflection of THz Radiation by a Superlattice. Physical Review Letters, 79(18), 3494-3497.

Hyart, T., Alekseev, K. N., & Thuneberg, E. V. (2008). Bloch Gain in dc-ac-driven semiconductor superlattices in the absence of electric domains. Physical Review B, 77(16), 165330-165342.

Hyart, T., Alexeeva, N. V., Mattas, J., & Alekseev, K. N. (2009). Possible Hz Bloch gain in dc-ac-driven superlattices. Microelectronics Journal, 40(4-5), 719–721.

Kroemer, H. (2000). Large-amplitude oscillation dynamics and domain suppression in a superlattice Bloch oscillator. Bell System Technical Journal, 1-21.

Litvinov,V. I., & Manasson, A. (2004). Large-signal negative dynamic conductivity and high-harmonic oscillations in a superlattice. Physical Review B, 70(19), 195323-195327.

Lurov, A., Gumbs, G., Roslyak, O., & D., H. (2011). Anomalous Photon-Assisted Tunneling in Graphene. Journal of Physics of Condensed Matter, 24(1), 1-8.

Musa, R., Mensah, S. Y., & Abukari, S. S. (2012). Photon-Assisted Process and High-Harmonic Dynamic Localization in Graphene Nanoribbons. arXiv preprint arXiv:1202.3469, 1-10.

Romanov,Y.A.,Romanova,Y. J., & G., M. L. (2009). Electron Bloch Oscillations and Electromagnetic Transparency of Semiconductor Superlattices in Multi-Frequency Electric Fields. Physical Review B, 79(24), 245321-245338.

Seidu,S.S. (2011).GENERATION AND AMPLIFICATION OF TERAHERTZ RADIATION IN CARBON NANOTUBES.Cape Coast: The University of Cape Coast, Department of Physics.

Son,Y. .,Cohen, M. L., & Louie, S. G. (2006). Half-Metallic Graphene Nanoribbons. Nature, 444(7117), 347-349.

Trauzettel, B., Blanter, Y. M., & Morpurgo, A. F. (2007). Photon-assisted electron transport in graphene: Scattering theory analysis. Physical Review B, 75(3), 0353051-0353055.

Yan, W. X., Bao, S. Q., & Zhao, X. G. (1998). Dynamic localization versus photon-assisted transport in semiconductor superlattices driven by dc-ac fields. Physical Review B, 7269-7272.

Zeuner, S. A. (1996). Photon-assisted Tunneling in GaAs/AlGaAs Superlattices up to Room Temperature. Applied Physics Letters, 69(18), 2689-2691.

Zhao, X. G. (1991). Dynamic localization conditions of a charged particle in a dc-ac electric field. Physics Letters A, 155(4-5), 299-302.